Selective Ion Penetration of Graphene Oxide Membranes

Pengzhan Sun,[†] Miao Zhu,[†] Kunlin Wang,[†] Minlin Zhong,[†] Jinquan Wei,[†] Dehai Wu,[†] Zhiping Xu,[‡,§] and Hongwei Zhu[†,§,*]

[†]Department of Mechanical Engineering, Key Laboratory for Advanced Manufacturing by Materials Processing Technology, [‡]Department of Engineering Mechanics, and [§]Center for Nano and Micro Mechanics (CNMM), Tsinghua University, Beijing 100084, China

ABSTRACT The selective ion penetration and water purification properties of freestanding graphene oxide (GO) membranes are demonstrated. Sodium salts permeated through GO membranes quickly, whereas heavy-metal salts infiltrated much more slowly. Interestingly, copper salts were entirely blocked by GO membranes, and organic contaminants also did not infiltrate. The mechanism of the selective ion-penetration properties of the GO membranes is discussed. The nanocapillaries formed within the membranes were responsible for the permeation of metal ions, whereas the coordination between heavy-metal ions with the GO membranes restricted the passage of the ions. Finally, the penetration processes of hybrid aqueous solutions were investigated; the results revealed that sodium salts can be separated effectively from copper salts and organic contaminants. The presented results demonstrate the potential applications of GO in areas such as barrier separation and water purification.

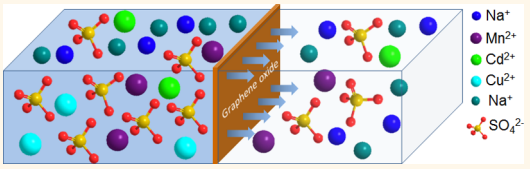

KEYWORDS: graphene oxides · ion penetration · water treatment

Currently, the rapid advancement of urbanization and industrialization has caused a lack of clean and safe water resources to be one of the most pervasive worldwide problems.[1] A growing number of contaminants are being poured into freshwater resources, which has led to numerous people becoming sick or dying from contaminated water and from water shortages. These problems have driven rapid advancements in water purification[1] and wastewater reutilization[2] in recent years. Graphene,[3] which is a new type of two-dimensional nanomaterial that consists of sp^2-hybridized carbon atoms arranged within a honeycomb-like network, has generated an extraordinary significant amount of interest due to its extraordinary properties. Researchers are now examining its potential applications in the treatment and reuse of wastewater. Graphene oxide (GO),[4−6] which is prepared by the chemical exfoliation of graphite, has been demonstrated to be another type of promising nanomaterial because of its advantages, which include its ease of synthesis and ease of scale-up. Furthermore, GO can be manipulated in aqueous solution and reassembled into large-area films with controlled thickness through methods such as drop-casting, spin-coating, vacuum filtration, electrostatic self-assembly, *etc.*[7] Once reassembled, the strong hydrogen bonds within the individual GO sheets hold the sheets together to form a lamellar structure. Because of the presence of oxygen-containing functional groups and adsorbed water molecules on both sides of the basal plane, the interlayer distance of the lamellar GO film is significantly larger than that of a multilayer stack of graphene.

GO sheets can be considered as graphene sheets asymmetrically decorated with oxygen-containing functional groups on the edges and the basal planes, which results in small sp^2 clusters isolated within the sp^3 matrix.[8] These oxygen-containing functional groups (hydroxyl and epoxy groups on the surface; carboxyl, carbonyl, phenol, *etc.* on the edges)[9] facilitate the interaction of GO sheets with a wide variety of organic and inorganic materials.

Recently, the penetration properties of graphene and GO films have been investigated. A single-layer graphene film has been demonstrated to be impermeable to gases and liquids, which is the thinnest membrane with the ability to separate two different phases.[10] The selective penetration properties of nanoporous graphene membranes have been investigated, and these investigations have revealed that

* Address correspondence to hongweizhu@tsinghua.edu.cn.

Received for review September 27, 2012 and accepted December 7, 2012.

Published online December 07, 2012
10.1021/nn304471w

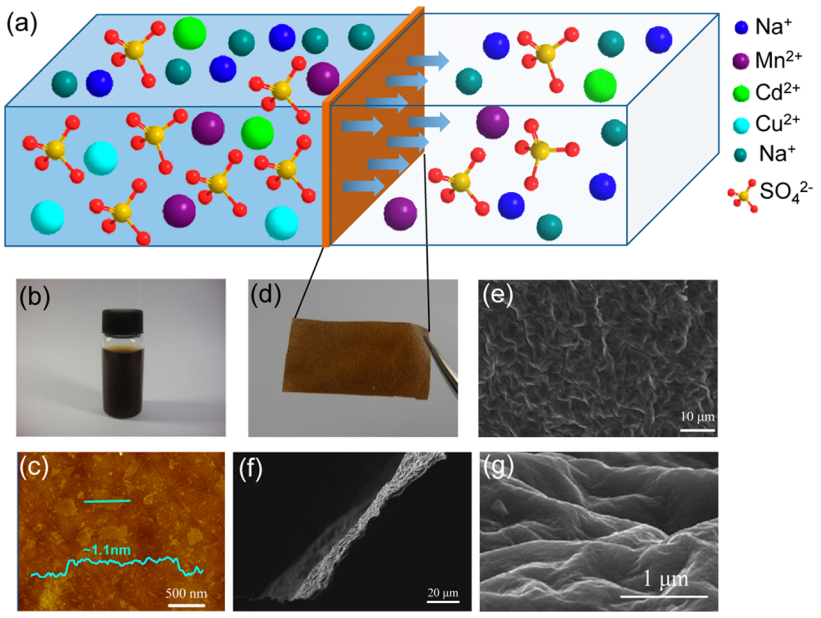

Figure 1. (a) Schematic diagram of the penetration processes of different ions through GO membranes. (b) GO colloidal suspension (2 mg/mL) used in the penetration experiments. (c) AFM image of the GO flakes; the inset shows the height profile of a layered GO sheet. (d) Photograph of a freestanding GO membrane prepared by drop-casting of a 2 mg/mL GO suspension. SEM images of (e) the surface and (f) a cross-section of the GO membrane. (g) The enlarged view of panel f.

nanoporous graphene films can be utilized to selectively separate different gases[11] and ions[12] through the design of various nanopores with different shapes, sizes, and chemical functionalities. Water desalination across nanoporous graphene has also been investigated.[13] The results of molecular dynamics simulations have indicated that single-layer graphene with nanopores can be utilized to separate NaCl from water efficiently and that the desalination performance depends on the pore size, chemical functionalization, and the pressure applied. These results make nanoporous graphene a promising material for use in high-performance membranes for water purification. A breakthrough in the penetration properties of GO films has recently been achieved,[14] where GO films have been shown to allow unimpeded percolation of water while blocking the penetration of other liquids, vapors, and gases.

Although the existing reports have demonstrated the potential applications of nanoporous graphene films in fields such as gas[11] and ion[12] separation as well as water desalination[13] assisted by molecular dynamics (MD) simulations, the realization of an experimental operation is difficult because large-area, high-quality, single-crystal graphene membranes with high mechanical strength have not thus far been synthesized. In addition, the immature techniques of introducing nanopores into graphene result in irregular pores, which will lead to the breakdown of graphene membranes during the application of high pressure due to stress concentration. However, the GO films prepared by drop-casting, spin-coating, and vacuum filtration methods are different. The strong hydrogen bonds hold the individual sheets within the GO films together, which endows the GO films with sufficient mechanical strength to make them freestanding and suitable for utilization in experimental operations. Furthermore, the oxygen-containing functional groups decorated asymmetrically on both sides of the GO sheets maintain both a relatively large interlayer distance and empty spaces between nonoxidized regions, which results in the formation of a network of nanocapillaries within the GO films. Water is allowed to permeate through these nanocapillaries smoothly, whereas other liquids, gases, and vapors are blocked.[14] Because a wide variety of organic and inorganic materials can interact with the oxygen-containing functional groups on the GO sheets in different manners, we have investigated the penetration behavior of different ions and molecules in aqueous solutions for the potential application of such GO films in fields such as barrier separation and water purification.

In this work, the selective penetration and water purification properties of GO membranes prepared by a simple drop-casting method are demonstrated, as illustrated in Figure 1a. The penetration properties of sodium salts, heavy-metal salts, organic contaminants (*e.g.*, rhodamine B) and a mixture of their aqueous solutions are investigated. The mechanism of the selective penetration properties of the GO membranes is discussed. These properties make GO a promising candidate in applications such as barrier separation and water purification.

RESULTS AND DISCUSSION

GO Membranes. GO flakes were prepared *via* a modified Hummer's method using worm-like graphite as

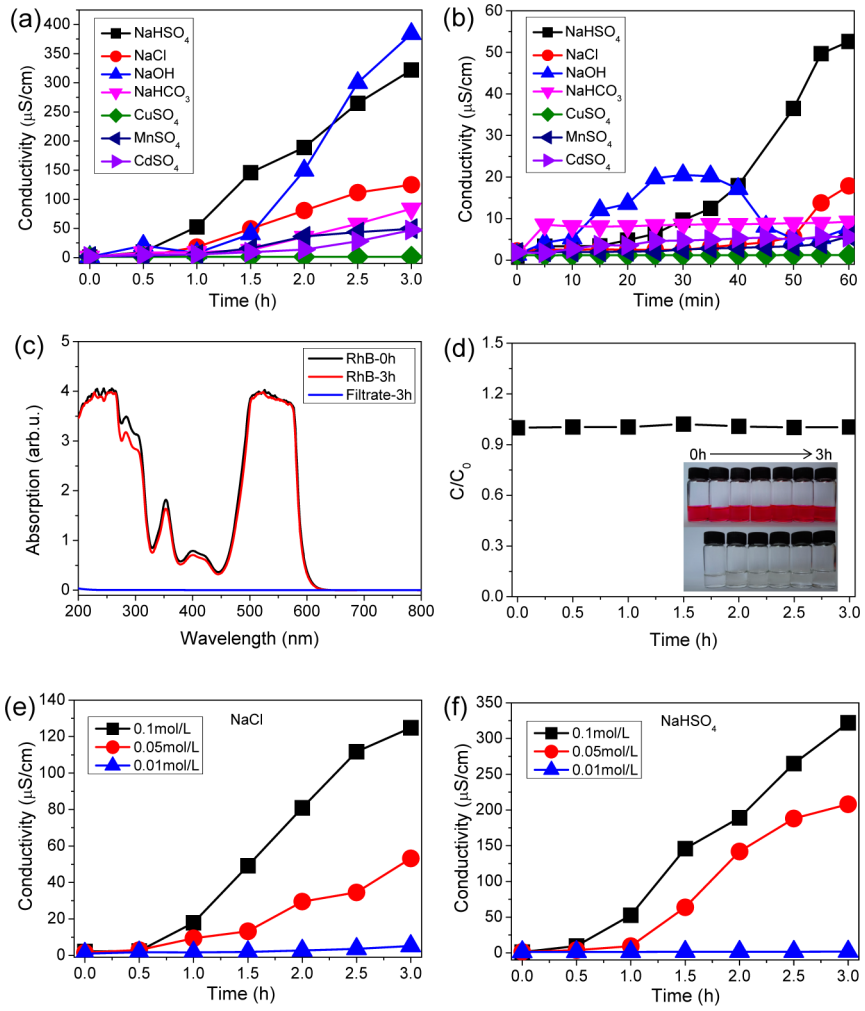

Figure 2. (a) The penetration processes of different ionic compounds through GO membranes. (b) The initial stages of the penetration processes. (c) UV−vis absorption spectra of a RhB suspension (0.1 mg/mL) and its filtrate after 3 h of penetration. (d) The relative concentration (C/C_0) change of the RhB suspension during the 3 h of penetration. The inset shows the corresponding photographs. The penetration processes of different concentrations of (e) NaCl and (f) $NaHSO_4$ solutions through GO membranes.

the source.[15] Figure 1b shows a photograph of a 2 mg/mL GO colloidal suspension. The AFM image of the as-prepared GO flakes is shown in Figure 1c. The image reveals that the synthetic GO sheets possess a lateral size of several hundred nanometers. The corresponding height profile reveals the monolayer nature of the as-prepared GO sheets.

Freestanding GO membranes were prepared by a simple drop-casting method. The preparation procedure is described as follows: ~1 mL of GO colloidal suspension (2 mg/mL) was drop-cast onto a piece of smooth paper and allowed to dry in air at room temperature. A piece of freestanding GO film was subsequently peeled from the underlying paper. A typical photograph of the as-prepared freestanding GO membrane is shown in Figure 1d, which reveals the large area, uniformity, and excellent mechanical strength of the GO membrane. SEM characterizations of the surface morphology and cross-section of the membranes are shown in Figure 1 panels e−g, which reveal that the as-prepared GO membranes possess a wrinkled surface topography and a lamellar structure. The membrane thickness was less than 10 μm, as shown in Figure 1f. The laminated structure of the freestanding GO membrane was further investigated using low-angle XRD, as shown in Supporting Information, Figure S1. The diffraction peak was located at $2\theta = 10.8°$, which corresponds to an intersheet spacing of 0.82 nm. More detailed SEM and AFM characterizations of as-prepared GO membranes are shown in Supporting Information, Figure S2.

Ion-Penetration. A series of ion-penetration experiments were conducted with a homemade plastic sink separated by a plastic plate, as shown in the schematic diagram of Figure 1a (see Methods for details). The selective ion-penetration properties obtained from different metallic salt solutions and from an organic contaminant (rhodamine B) are shown in Figure 2. The conductivities of all the metallic salt solutions with a concentration of 0.1 mol/L were in the range

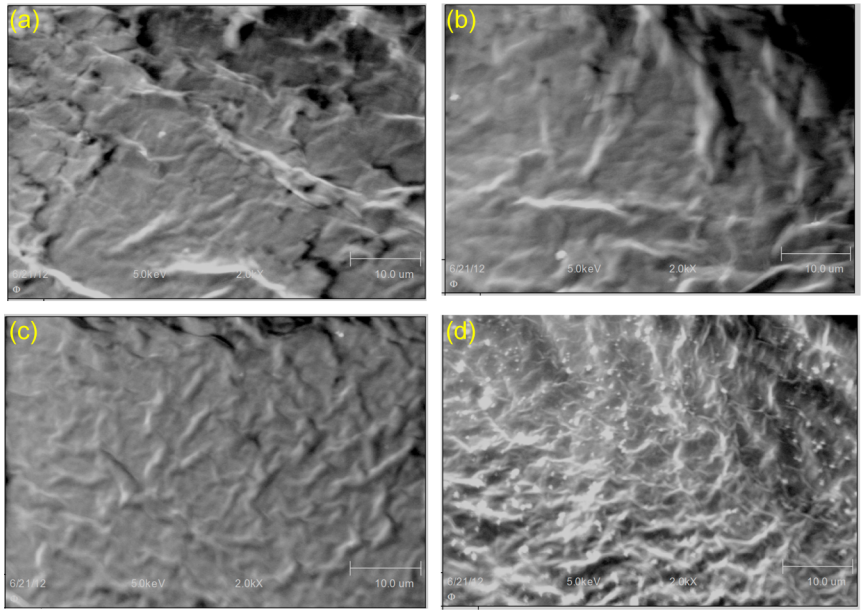

Figure 3. SEM images of GO membranes after 3 h of penetration by (a) $NaHSO_4$, (b) NaCl, (c) $NaHCO_3$, and (d) $CuSO_4$.

of 6−29 mS/cm, whereas the conductivities of all the filtrates were on the order of μS/cm. The conductivities of the filtrates directly reflected their concentration. As shown in Figure 2a, the conductivities of all 0.1 mol/L metallic salt solutions exhibited similar tendencies. In the initial stage, the conductivity changed little, whereas it increased significantly in a near-linear manner afterward. The permeability of different metallic salt solutions changed dramatically. The sodium salts permeated efficiently through the GO membrane, whereas the heavy-metal salts infiltrated much more slowly. In addition, strong acids and bases exhibited greater permeabilities than did normal salts, whereas basic salts (*e.g.*, $NaHCO_3$), which reacted with the functional groups on GO sheets and produced gases, exhibited relatively lower permeabilities. Interestingly, copper sulfate was blocked entirely by the GO film, and the conductivity of the filtrate remained almost unchanged (*i.e.*, the conductivity remained the same as that of the deionized water). The stages in which initial conductivity changed are shown in Figure 2b, which reveals that the filtrates' conductivities changed slightly except for that of the $NaHSO_4$ aqueous solution. A peak was also observed in the initial conductivity change stage of the NaOH solution, which can be attributed to the reaction between NaOH and the functional groups decorated on both sides of the GO sheets. To compare the permeation rates of different metallic salts through the GO membranes, relative conductivities (defined as the conductivity of the filtrate divided by that of a 0.1 mol/L initial aqueous solution) were considered, as shown in Supporting Information, Figure S3. The results reveal that the relative conductivities of the different metallic salts changed significantly. Sodium salts permeated faster than heavy-metal salts. The sodium salts with different anion radicals exhibited different penetration rates in the approximate order NaOH > $NaHSO_4$ > NaCl > $NaHCO_3$.

For the 0.1 mg/mL rhodamine B aqueous solution, the UV−vis absorption spectra of the filtrate and solutions were investigated before and after 3 h of penetration, as shown in Figure 2c. The filtrate exhibited no absorption peak in the tested range of 200−800 nm, whereas the absorption peaks of the rhodamine B solutions before and after 3 h of penetration nearly overlap, which indicates that organic contaminants such as rhodamine B cannot infiltrate through GO membranes. In Figure 2d, the relative concentration (C/C_0) of the rhodamine B solution, which is represented by the absorption peak intensity ratio at 552 nm, is plotted; the plots demonstrate the nearly constant concentration of rhodamine B during 3 h of penetration. The inset in Figure 2d also reveals the unchanged color of the rhodamine B solutions and the corresponding filtrates during penetration, which further suggests the effective resistance of the GO membranes to organic contaminants.

The penetration properties of NaCl and $NaHSO_4$ solutions of different concentrations were investigated, as shown in Figure 2e,f. As the concentration of NaCl and $NaHSO_4$ solutions were decreased, the permeability decreased. When the concentration was decreased to a certain critical value, the metallic salts could not infiltrate through the GO films.

Typical SEM characterizations of GO membranes after penetration for $NaHSO_4$, NaCl, $NaHCO_3$, and $CuSO_4$ are shown in Figure 3a−d. The results reveal that, after 3 h of penetration, the GO membrane still possessed a continuous structure. The membranes

after the penetration of $NaHSO_4$, NaCl, and $NaHCO_3$ showed no difference when compared with the original ones, whereas, after the penetration of $CuSO_4$, a large number of nanoparticles adhered to the GO surface. The XPS study for Cu 2p (Supporting Information, Figure S4) reveal four main peaks located at 933.6, 943.2, 953.4, and 962.5 eV; these peaks are characteristic of the Cu^{2+} state.[16] We therefore attribute the formation of these nanoparticles to the "post-crystallization" of $CuSO_4$ after the GO membrane had dried up.

Mechanism and Model. The mechanism of the selective penetration properties of the GO membranes was investigated. As shown in Supporting Information, Figure S5, the hydrophilicities (contact angles) of different aqueous solutions on the GO membranes were investigated, and the results demonstrate that all of the aqueous solutions exhibited approximately the same hydrophilicity on membranes as did H_2O, which indicates that the differences in hydrophilicity are not responsible for the selective penetration of the GO membranes. In addition, the energy-dispersive spectroscopy (EDS, Supporting Information, Figure S6) results demonstrate that small amounts of metallic salts remained in the GO membranes after the salts were permeated through the membranes for 3 h. Supporting Information, Figure S7 shows the X-ray photoelectron spectroscopy (XPS) results for the GO membranes after the penetration experiments. After the penetration of $NaHSO_4$, the C1s binding energies of the membranes still exhibited three typical peaks located at 284.6, 286.9, and 288.7 eV, which correspond to C−C bonds, epoxy/ether groups, and carboxyl groups, respectively; the XPS spectra of this sample was identical to that of the initial GO membranes (Supporting Information, Figure S7a). However, after the films were penetrated by the other aqueous solutions, a new peak appeared in the C 1s binding energy at ~283 eV, which was attributed to the interaction between the metal ions and the carbon atoms within the GO sheets. In the case of $NaHSO_4$, the peak at ~283 eV most likely disappeared because a large amount of H^+ ions exists in $NaHSO_4$ aqueous solutions, which prevents the interaction between carbon atoms and Na^+ ions. In addition, these H^+ ions inhibit the ionization of oxygen-containing functional groups, which results in the invariability of carboxyl-group binding energies of GO membranes. In contrast, in the cases of other aqueous solutions, the C1s binding energies that correspond to carboxyl groups shift to lower energies due to the ionization of functional groups on the GO surfaces. The XPS results indicate that the selective penetration properties of GO membranes can be attributed to the different interaction strengths between metal ions and GO membranes. The distribution of metallic salts within the GO membranes after penetration was investigated using Auger electron spectroscopy (AES), as shown in Supporting Information, Figure S8. The results reveal that the concentrations of all of the metallic salts that remained within the GO membranes were less than 10%, which indicates that a very low level of sorption was maintained. Notably, in the range of the depth investigated, the concentrations of C and Na were approximately symmetrical along the dashed line shown in Figure S8a−c. This result reveals that, when the concentration of C was greater, the concentration of Na became symmetrically lower. However, in Figure S8d, the distribution of the concentrations of C and Cu no longer show a symmetrical nature. These results indicate that, during the penetration processes, Na^+ ions were intercalated between the GO layers to form ordered Na^+ ions layers, whereas the Cu^{2+} ions distributed randomly within the GO membranes, which led to the nearly constant distribution of Cu^{2+} ions in the investigated range of depths.

On the basis of the previously discussed experimental results, we propose a theoretical model for the selective penetration properties of GO membranes (Figure 4). Within the GO membranes fabricated *via* the drop-casting method, GO sheets with lateral sizes of several hundred nanometers stack together to form a lamellar structure (Figure 1f,g). According to previous results,[14] the oxygen-containing functional groups tend to cluster together, which leaves other nonoxidized regions to form a two-dimensional network of graphene nanocapillaries (Figure 4a). These nanocapillaries provide high capillary pressures, which facilitates the low-friction flow of water, whereas water molecules within the oxidized regions exhibit poor mobility due to the interaction of hydrogen bonding and functional groups.[14] When the distance between GO interlayers becomes sufficiently large, the nanocapillaries allow the permeation of hydrated ions (Figure 2 and Supporting Information, Figure S3). However, the selectivity of the GO membranes cannot be explained solely by ionic-radius-based theories. For example, the relative penetration ability of the studied metallic ions follows the approximate order of $Na^+ > Mn^{2+} > Cd^{2+} > Cu^{2+}$ (Figure 2a and Supporting Information, Figure S3), even though the radii of these naked and hydrated ions arrange in the order of $Mn^{2+} > Cd^{2+} > Cu^{2+} > Na^+$. Because a large number of oxygen-containing functional groups decorate the surfaces and edges of the GO sheets, the GO sheets can be regarded as large organic molecules. The electrostatic attractions and chemical interactions between these functional groups and hydrated ions are responsible for the selective penetration properties of GO membranes.

During the penetration process, a GO membrane is first wetted by the aqueous solution, and the distances between the interlayers become gradually larger during this process. According to the XRD results (Supporting Information, Figure S1), the diffraction peak of the as-prepared GO membrane was located

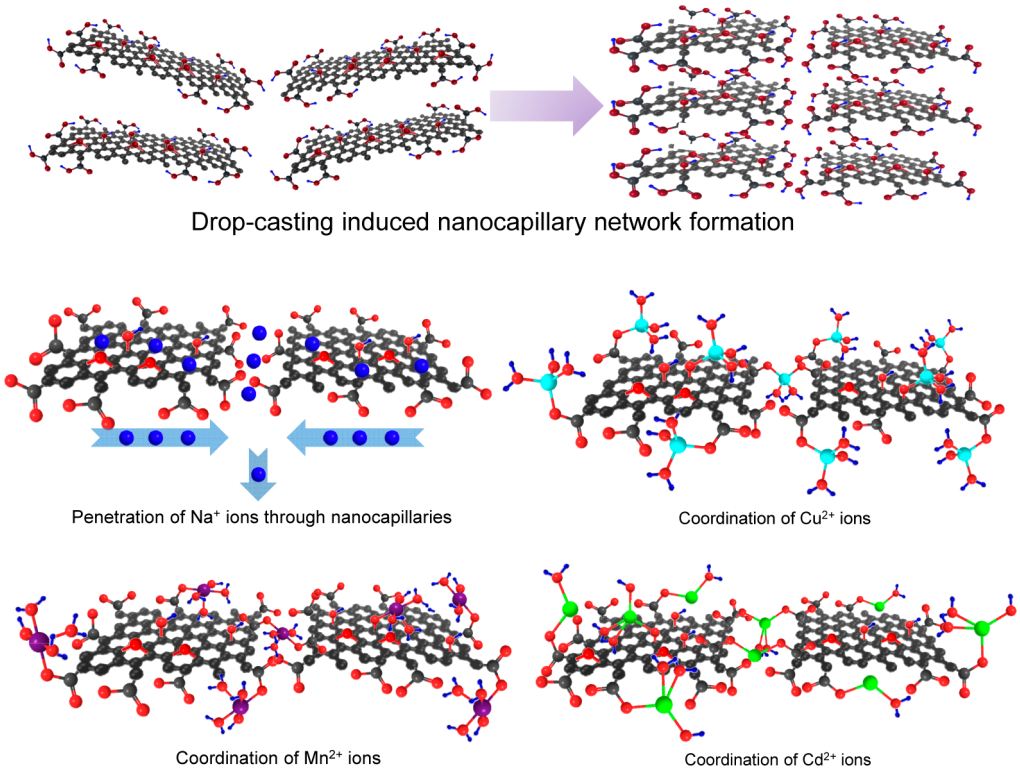

Figure 4. Schematic diagrams of GO membrane and the interaction with different ions.

at $2\theta = 10.8°$, which corresponds to an interlamellar spacing of ~0.8 nm. This distance allows water molecules to fill the nanocapillaries and permeate to the other side of the GO membrane.[14] However, such a distance is still not sufficiently large to allow the penetration of hydrated ions. As the GO membrane is wetted, the interlayer spacing becomes larger. Finally, the spacing becomes sufficiently large for the hydrated ions to fill the nanocapillaries and migrate to the other side under the high capillary pressures. This mechanism explains why the conductivities of the filtrates change little at first and then increase significantly faster afterward (shown in Figure 2 and Supporting Information, Figure S3). During the process of iontophoretic injection, anions permeate through the nanocapillaries more easily than do cations because of the strong repulsive forces between the cations and the functional groups.

For the aqueous solutions of sodium salts, the Na^+ ions are highly ionic; they are consequently not constrained to bind with the oxygen-containing functional groups, such as carboxylate and hydroxyl groups.[17] However, different types of anions in the aqueous solutions significantly change the penetration nature of sodium salts. For example, in the case of the NaOH solution, the intensive reactions between OH^- ions and carboxyl and hydroxyl groups make the GO sheets highly ionic and chemically active. The interlayer distance increases, and the nanocapillaries become much looser, which leads to a fast penetration of Na^+ ions and OH^- ions. In contrast, in the case of the $NaHSO_4$ solution, the H^+ ions prohibit the ionization of the oxygen-containing functional groups, and no chemical reactions occur between the ions in the aqueous solution and the functional groups. On the basis of this reasoning, the penetration rate of $NaHSO_4$ is significantly lower. However, because hydrated H^+ ions are significantly smaller than hydrated Na^+ ions, hydrated H^+ ions can penetrate through the nanocapillaries more easily, which leads to the relative higher conductivity of the $NaHSO_4$ filtrate compared to that of the NaCl filtrate (Figures 2 and S3). With respect to the $NaHCO_3$ solution, the chemical reactions between the HCO_3^- ions and the carboxyl groups lead to the generation of CO_2 gas, which was observed directly during the penetration experiments. Although these chemical reactions result in the ionization of GO sheets, the production of gases within the nanocapillaries results in the generation of a reversed compression, which suppresses the permeation of ions. Consequently, the conductivity of the $NaHCO_3$ filtrate was relatively less than that of the NaCl filtrate (Figure 2 and Supporting Information, Figure S3). On the basis of this point of view, the order of the penetration ability of sodium salts in the aqueous solutions decreases in the approximate order NaOH > $NaHSO_4$ > NaCl > $NaHCO_3$, which is in good agreement with the ion-penetration results shown in Figure 2 and Supporting Information, Figure S3.

The penetration abilities of aqueous solutions of heavy-metal salts (*e.g.*, $MnSO_4$, $CdSO_4$, and $CuSO_4$), are

significantly lower than those of the alkali salts (Figure 2 and Supporting Information, Figure S3), which is due to the tight coordination between the heavy-metal ions and the functional groups decorated on the GO sheets as shown in Figure 4. Among the three studied heavy-metal ions, Cu^{2+} ions favor square-planar coordination geometry,[18] the soft-metal Cd^{2+} ions favor linear or tetrahedral coordination,[18,19] and the Mn^{2+} ions favor trigonal-bipyramidal geometry.[19] The previously discussed results indicate that the oxygen-containing functional groups can easily substitute water molecules from the hydrated complex because water molecules do not contain the functional groups needed to strengthen the bond to a metal ion and because the interaction energies of negatively charged functional groups are significantly greater than those of neutral functional groups.[18] In the case of Cu^{2+} and Cd^{2+} ions, the Cu^{2+} is a d^9 ion, and its complexes possess a doublet ground state; in contrast, the Cd^{2+} is a d^{10} ion, and its complexes possess a singlet ground state.[18] With respect to the coordination of ions with oxygen-containing functional groups (*e.g.*, carboxylate groups), the Cu^{2+} ions tend to bind in a *syn* conformation, whereas Cd^{2+} ions are more likely to bind in a direct conformation, where they share two carboxylate oxygen atoms equally.[17] These differences in coordination conformation result in a smaller average distance between Cu^{2+} ions and carboxylate groups than that of Cd^{2+} ions, indicating a larger binding energy of Cu^{2+}-O than that of Cd^{2+}-O. The previous calculation results also revealed that the relative affinity of Cu^{2+} ions is significantly greater than that of Cd^{2+} ions in the cases of $-O^-$ and $-COO^-$ functional groups,[18] which indicates that the interaction energies of Cu^{2+} ions that coordinate to oxygen-containing functional groups on GO sheets are greater than those of Cd^{2+} ions, leading to the weaker penetration ability of Cu^{2+} than that of Cd^{2+} (Figure 2 and Supporting Information, Figure S3). In contrast with Cu^{2+} ions, the Mn^{2+} ions are more likely to bind to carboxylate groups in an *anti* conformation,[17] which is less stable than the *syn* conformation. This difference leads to a larger average distance of Mn^{2+}-O bonds than that of Cu^{2+}-O bonds, indicating the smaller binding strength of Mn^{2+}-O compared to the Cu^{2+}-O bonds. Moreover, in the case of Cu^{2+} complexes, the overlap between the 2p orbital of oxygen atoms and the hybrid sd orbitals of Cu^{2+} ions makes a covalent contribution to the interaction between Cu^{2+} and the oxygen-containing functional groups,[18−20] whereas little covalent contribution is found for the Mn^{2+} ions because of their poor polarizability.[19] The covalent character leads to a greater affinity of Cu^{2+} ions for the oxygen-containing functional groups compared to that of Mn^{2+} ions. However, in aqueous environments, the coordination of water molecules to the metal ions causes a reduction in the binding energies because of the lack of orbital availability, and the different bond nature and the different coordination type, which results in a purely electrostatic bonding nature of the complexes.[19] Despite this fact, the binding energies of Cu^{2+} ions to oxygen-containing functional groups are still greater than those of Mn^{2+} ions, which is attributed to the internal polarizability of the complexes.[19] The above results lead to an enhanced permeation of Mn^{2+} than that of Cu^{2+} (Figure 2 and Supporting Information, Figure S3). Previous investigations on the sorption of heavy-metal ions from aqueous solutions by carbon nanotubes have suggested that the sorption processes are mainly attributed to the chemical interactions between the metal ions and the functional groups on the surfaces of the carbon nanotubes.[21] With respect to the Mn^{2+} and Cd^{2+} ions, previous adsorption experiments revealed that the affinity of Cd^{2+} ions to carbon nanotubes is greater than that of Mn^{2+} ions,[22] which indicates a stronger binding between Cd^{2+} ions and the functional groups on the surfaces of carbon nanotubes than that of Mn^{2+} ions. Because a larger amount of oxygen-containing functional groups are present on the surfaces of GO sheets compared to the surfaces of carbon nanotubes, the interactions between Cd^{2+} ions and the GO sheets are believed to be significantly stronger than the interactions between Mn^{2+} ions and the GO sheets. In summary, the penetration ability of the studied heavy-metal ions (Cu^{2+}, Mn^{2+}, and Cd^{2+}) through GO membrane follows the order $Mn^{2+} > Cd^{2+} > Cu^{2+}$, which is in consistent with the experimental results (Figure 2a and Supporting Information, Figure S3).

In the case of the RhB aqueous solution, the RhB molecules can be effectively captured by GO sheets because of the positively charged nature and $\pi-\pi$ stacking interactions, which result in the tight binding between the RhB molecules and the GO sheets (Figure 2c,d).[23]

Barrier Separation Ability. Finally, the barrier separation ability of GO membranes was investigated based on mixtures of $CuSO_4$ (0.1 mol/L)−NaCl (0.1 mol/L) and NaCl (0.1 mol/L)−RhB (0.1 mg/mL) aqueous solutions, as shown in Figure 5. The changes in conductivities measured for the filtrates of the mixture solutions exhibited the same tendencies. At the initial stage, the conductivities changed slightly, whereas the conductivities increased dramatically in a near-linear manner afterward, as shown in Figure 5a,b. This behavior occurs because, at the initial stage, the GO membranes undergo a wetting stage, where the expansion of the interlayer distances causes an enlargement of the nanocapillaries. When the nanocapillaries become sufficiently large, the hydrated Na^+ ions are able to penetrate the membrane with the aid of high capillary pressure, which leads to the linear increase in the conductivities. However, the variations in the amplitudes of the conductivities of the mixture solutions

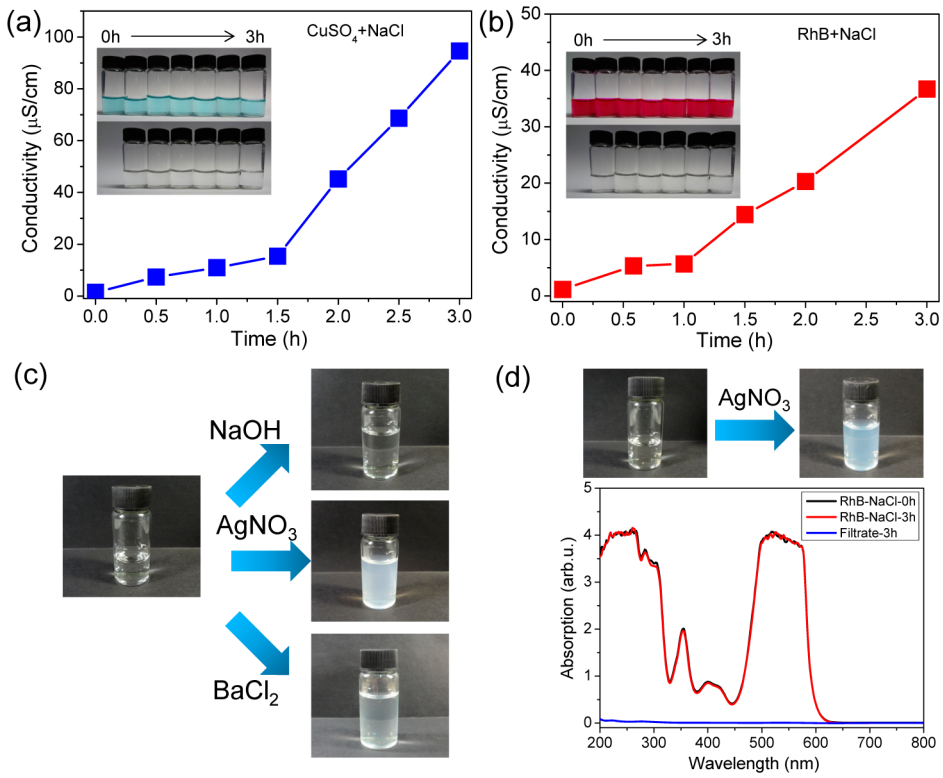

Figure 5. (a) The penetration process of a mixture of $CuSO_4$ (0.1 mol/L) and NaCl (0.1 mol/L). The inset shows the photographs of the mixture and its filtrates during 3 h of penetration. (c) The corresponding filtrates before and after NaOH, $AgNO_3$, and $BaCl_2$ were added. (b) The penetration process of a mixture of RhB (0.1 mg/mL) and NaCl (0.1 mol/L). The inset shows the photographs of the mixture and its filtrates during 3h of penetration. (d) UV–vis adsorption spectra of the mixture and its filtrates after 3h of penetration. The inset above shows the filtrates before and after $AgNO_3$ was added.

were smaller than that of the pure NaCl solution, which is attributed to the enhanced interactions between ions in the solutions that block the penetration of Na^+ and Cl^- ions. Moreover, the coordination of carboxylate groups on neighboring GO sheets with the same copper ions and RhB molecules may partially block nanocapillaries and decrease the penetration ability of Na^+ and Cl^- ions. The insets of Figure 5a,b reveal that the colors of the $CuSO_4$ and RhB solutions as well as those of their filtrates remained unchanged during the 3 h penetration process, which further demonstrates the effective prohibition of the penetration of copper sulfate and RhB through the GO membranes. To the filtrates of the $CuSO_4$ and NaCl mixture solution after 3 h of penetration was added the same volume of 0.1 mol/L NaOH, $AgNO_3$ and $BaCl_2$ solutions to demonstrate the existence or absence of Cu^{2+}, Cl^-, and SO_4^{2-} ions in the filtrates. The corresponding photographs are shown in Figure 5c. After the addition of NaOH solution, no precipitates were observed in the filtrate, which indicated the absence of Cu^{2+} ions. In contrast, the filtrates of solutions to which $AgNO_3$ and $BaCl_2$ were added contained white precipitates, which indicated the presence of Cl^- and SO_4^{2-}. The amount of precipitate in the filtrate of the solution that contained added $AgNO_3$ was greater than that of the solution that contained added $BaCl_2$; this result reflected the larger amount of Cl^- compared to the amount of SO_4^{2-}. In Figure 5d, the UV–vis absorption spectra of the filtrates and the RhB–NaCl mixture solutions before and after penetration for 3 h are presented. The absorption peaks of the filtrates were still absent in the tested range, and the absorption curves of the RhB solutions before and after penetration for 3 h nearly matched. After $AgNO_3$ solution was added to the filtrate, a significant amount of white precipitate appeared immediately, which demonstrated the successful penetration of Na^+ and Cl^- through the GO membranes and the effective prevention of the passage of RhB molecules. During the whole penetration process, the ions in the solutions permeated spontaneously through the GO membranes. Because of the different diameters of the ions in the solutions and because of the different interactions with GO membranes, different types of ions can be separated effectively when GO membranes are adapted as barrier membranes.

Problems Need to be Addressed. GO membranes prepared *via* the simple drop-casting method possess excellent properties, including easy scale-up, room-temperature preparation, and excellent mechanical strength, and they are conveniently functionalized. In addition, GO membranes contain a large number of nanocapillaries, which form a network to facilitate the penetration of water molecules and certain hydrated

ions. The oxygen-containing functional groups decorated on GO sheets facilitate the coordination with a variety of metal ions; these properties endow GO membranes with selective penetration properties and make them a promising candidate in future wastewater reuse and purification applications. However, some problems need to be addressed before the extensive application of GO membranes. For example, the GO membranes used in all of the penetration experiments conducted in this investigation possess a thickness of several micrometers (<10 μm). Thinner films exhibit poor mechanical strength, which is unfavorable for the use of free-standing membranes with aqueous solutions and makes them rather frangible. Therefore, the preparation of ultrathin free-standing GO membranes with excellent mechanical strength remains a major challenge. Fortunately, chemical cross-linking can significantly enhance the mechanical properties through coordination between the oxygen-containing functional groups and Ca^{2+} and Mg^{2+} ions.[24,25] Because the interactions between alkaline-earth metal ions and the functional groups on GO sheets can be significantly weakened under aqueous conditions because of their highly ionic nature, other divalent metal ions must be utilized to realize stable chemical cross-linking in solutions and to overcome minor obstacles to wanted molecules. The functionalization of GO membranes with different types of chelating ligands will result in complexes with many other toxic heavy-metal ions,[26] which will enlarge the application range of GO membranes with respect to ion selectivity. The exploration of potential applications in wastewater purification with functionalized GO membranes is now underway.

CONCLUSION

In summary, the selective ion penetration and water purification properties of freestanding GO membranes prepared *via* a simple drop-casting method were demonstrated. Sodium salts permeated quickly through the GO membranes, whereas heavy-metal salts infiltrated much more slowly. Copper sulfate and organic contaminants, such as rhodamine B, are blocked entirely because of their strong interactions with the GO membranes. The mechanism of the selective ion penetration properties of GO membranes was investigated systematically, and the nanocapillaries formed within lamellar structure and the different chemical interactions between the metal ions and the oxygen-containing functional groups were demonstrated to be responsible for the selective penetration properties of the GO membranes. The barrier separation experiments based on mixture solutions demonstrated the effective separation of sodium salts from copper sulfate and rhodamine B. Our results indicate that GO membranes are a promising candidate in future applications, such as barrier separation and wastewater purification.

METHODS

Preparation of GO Membranes. Natural graphite flakes were mixed with concentrated sulfuric acid and hydrogen peroxide, then stirred for 1 h and washed with deionized water until a pH of ~7 was reached. The obtained mixture was allowed to dry at 40 °C for 24 h and was then expanded through fast heating at 1000 °C for 10s to convert the graphite intercalation compounds into worm-like graphite. The worm-like graphite was further converted to graphite oxides *via* a modified Hummer's method, and the GO colloid suspension was obtained by sonication in water.

Ion-Penetration Test. The plate contained a hole with a diameter of 5 mm in its center, which was allowed to seal with a piece of freestanding GO membrane by a piece of double-sided copper tape. The tape contained a hole with the same diameter in the middle to ensure the GO membrane directly contacted the solutions in two separated sinks. One hundred milliliters of certain aqueous solutions and deionized water were injected into the two separated sinks with the same injection speed to ensure that the GO membrane bore the same pressure. The concentration of the filtrate was reflected by measuring its conductivity.

Conflict of Interest: The authors declare no competing financial interest.

Acknowledgment. This work is supported by the National Science Foundation of China (50972067), the Beijing Natural Science Foundation (2122027), the National Program on Key Basic Research Project (2011CB013000), and Tsinghua University Initiative Scientific Research Program (2012Z02102).

Supporting Information Available: Supplementary figures including XRD, AFM, SEM, XPS, EDX, and AES results. This material is available free of charge *via* the Internet at http://pubs.acs.org.

REFERENCES AND NOTES

1. Shannon, M. A.; Bohn, P. W.; Elimelech, M.; Georgiadis, J. G.; Marinas, B. J.; Mayes, A. M. Science and Technology for Water Purification in the Coming Decades. *Nature* **2008**, *452*, 301–310.
2. Logan, B. E.; Elimelech, M. Membrane-Based Processes for Sustainable Power Generation Using Water. *Nature* **2012**, *488*, 313–319.
3. Novoselov, K. S.; Geim, A. K.; Morozov, S. V.; Jiang, D.; Zhang, Y.; Dubonos, S. V.; Grigorieva, I. V.; Firsov, A. A. Electric Field Effect in Atomically Thin Carbon Films. *Science* **2004**, *306*, 666–669.
4. Stankovich, S.; Dikin, D. A.; Piner, R. D.; Kohlhaas, K. A.; Kleinhammes, A.; Jia, Y.; Wu, Y.; Nguyen, S. T.; Ruoff, R. S. Synthesis of Graphene-Based Nanosheets *via* Chemical Reduction of Exfoliated Graphite Oxide. *Carbon* **2007**, *45*, 1558–1565.
5. Eda, G.; Fanchini, G.; Chhowalla, M. Large-Area Ultrathin Films of Reduced Graphene Oxide as a Transparent and Flexible Electronic Material. *Nat. Nanotechnol.* **2008**, *3*, 270–274.
6. Ramanathan, T.; Abdala, A. A.; Stankovich, S.; Dikin, D. A.; Herrera-Alonso, M.; Piner, R. D.; Adamson, D. H.; Schniepp, H. C.; Chen, X.; Ruoff, R. S.; *et al.* Functionalized Graphene Sheets for Polymer Nanocomposites. *Nat. Nanotechnol.* **2008**, *3*, 327–331.
7. Eda, G.; Chhowalla, M. Chemically Derived Graphene Oxide: Towards Large-Area Thin-Film Electronics and Optoelectronics. *Adv. Mater.* **2010**, *22*, 2392–2415.

8. Loh, K. P.; Bao, Q.; Eda, G.; Chhowalla, M. Graphene Oxide as a Chemically Tunable Platform for Optical Applications. *Nat. Chem.* **2010**, *2*, 1015–1024.
9. Hontoria-Lucas, C.; López-Peinado, A. J.; López-González, J. d. D.; Rojas-Cervantes, M. L.; Martín-Aranda, R. M. Study of Oxygen-Containing Groups in a Series of Graphite Oxides: Physical and Chemical Characterization. *Carbon* **1995**, *33*, 1585–1592.
10. Bunch, J. S.; Verbridge, S. S.; Alden, J. S.; Zande, A. M.; Parpia, J. M.; Craighead, H. G.; McEuen, P. L. Impermeable Atomic Membranes from Graphene Sheets. *Nano Lett.* **2008**, *8*, 2458–2462.
11. Du, H.; Li, J.; Zhang, J.; Su, G.; Li, X.; Zhao, Y. Separation of Hydrogen and Nitrogen Gases with Porous Graphene Membrane. *J. Phys. Chem. C* **2011**, *115*, 23261–23266.
12. Sint, K.; Wang, B.; Kral, P. Selective Ion Passage through Functionalized Graphene Nanopores. *J. Am. Chem. Soc.* **2008**, *130*, 16448–16449.
13. Cohen-Tanugi, D.; Grossman, J. C. Water Desalination across Nanoporous Graphene. *Nano Lett.* **2012**, *12*, 3602–3608.
14. Nair, N. N.; Wu, H. A.; Jayaram, P. N.; Grigorieva, I. V.; Geim, A. K. Unimpeded Permeation of Water through Helium-Leak-Tight Graphene-Based Membranes. *Science* **2012**, *335*, 442–444.
15. Gu, W.; Zhang, W.; Li, X.; Zhu, H.; Wei, J.; Li, Z.; Shu, Q.; Wang, C.; Wang, K.; Shen, W.; *et al.* Graphene Sheets from Worm-like Exfoliated Graphite. *J. Mater. Chem.* **2009**, *19*, 3367–3369.
16. Espinós, J. P.; Morales, J.; Barranco, A.; Caballero, A.; Holgado, J. P.; González-Elipe, A. R. Interface Effects for Cu, CuO, and Cu_2O Deposited on SiO_2 and ZrO_2. XPS Determination of the Valence State of Copper in Cu/SiO_2 and Cu/ZrO_2 Catalysts. *J. Phys. Chem. B* **2002**, *106*, 6921–6929.
17. Carrell, C. J.; Carrell, H. L.; Erlebacher, J.; Glusker, J. P. Structural Aspects of Metal Ion−Carboxylate Interactions. *J. Am. Chem. Soc.* **1988**, *110*, 8651–8656.
18. Rulíšek, L.; Havlas, Z. Theoretical Studies of Metal Ion Selectivity. 1. DFT Calculations of Interaction Energies of Amino Acid Side Chains with Selected Transition Metal Ions (Co^{2+}, Ni^{2+}, Cu^{2+}, Zn^{2+}, Cd^{2+}, and Hg^{2+}). *J. Am. Chem. Soc.* **2000**, *122*, 10428–10439.
19. Marino, T.; Toscano, M.; Russo, N.; Grand, A. Structural and Electronic Characterization of the Complexes Obtained by the Interaction between Bare and Hydrated First-Row Transition-Metal Ions (Mn^{2+}, Fe^{2+}, Co^{2+}, Ni^{2+}, Cu^{2+}, Zn^{2+}) and Glycine. *J. Phys. Chem. B* **2006**, *110*, 24666–24673.
20. Bala, T.; Prasad, B. L. V.; Sastry, M.; Kahaly, M. U.; Waghmare, U. V. Interaction of Different Metal Ions with Carboxylic Acid Group: A Quantitative Study. *J. Phys. Chem. A* **2007**, *111*, 6183–6190.
21. Rao, G. P.; Lu, C.; Su, F. Sorption of Divalent Metal Ions from Aqueous Solution by Carbon Nanotubes: A Review. *Sep. Purif. Technol.* **2007**, *58*, 224–231.
22. Liang, P.; Liu, Y.; Guo, L.; Zeng, J.; Lu, H. Multiwalled Carbon Nanotubes as Solid-Phase Extraction Adsorbent for the Preconcentration of Trace Metal Ions and Their Determination by Inductively Coupled Plasma Atomic Emission Spectrometry. *J. Anal. At. Spectrom.* **2004**, *19*, 1489–1492.
23. Yang, S.; Chen, S.; Chang, Y.; Cao, A.; Liu, Y.; Wang, H. Removal of Methylene Blue from Aqueous Solution by Graphene Oxide. *J. Colloid Interface Sci.* **2011**, *359*, 24–29.
24. Park, S.; Lee, K.-S.; Bozoklu, G.; Cai, W.; Nguyen, S. T.; Ruoff, R. S. Graphene Oxide Papers Modified by Divalent Ions—Enhancing Mechanical Properties *via* Chemical Cross-Linking. *ACS Nano* **2008**, *2*, 572–578.
25. Liu, Y.; Xie, B.; Xu, Z. Mechanics of Coordinative Crosslinks in Graphene Nanocomposites: a First-Principles Study. *J. Mater. Chem.* **2011**, *21*, 6707–6712.
26. Yan, L.; Zheng, Y.; Zhao, F.; Li, S.; Gao, X.; Xu, B.; Weiss, P. S.; Zhao, Y. Chemistry and Physics of a Single Atomic Layer: Strategies and Challenges for Functionalization of Graphene and Graphene-Based Materials. *Chem. Soc. Rev.* **2012**, *41*, 97–114.